nature biotechnology

# Induction of functional dopamine neurons from human astrocytes *in vitro* and mouse astrocytes in a Parkinson's disease model

Pia Rivetti di Val Cervo[1], Roman A Romanov[2,3], Giada Spigolon[3], Débora Masini[3], Elisa Martín-Montañez[1,4], Enrique M Toledo[1], Gioele La Manno[1], Michael Feyder[3], Christian Pifl[2], Yi-Han Ng[5], Sara Padrell Sánchez[1], Sten Linnarsson[1], Marius Wernig[5], Tibor Harkany[2,3], Gilberto Fisone[3] & Ernest Arenas[1]



**Cell replacement therapies for neurodegenerative disease have focused on transplantation of the cell types affected by the pathological process. Here we describe an alternative strategy for Parkinson's disease in which dopamine neurons are generated by direct conversion of astrocytes. Using three transcription factors, NEUROD1, ASCL1 and LMX1A, and the microRNA miR218, collectively designated NeAL218, we reprogram human astrocytes *in vitro*, and mouse astrocytes *in vivo*, into induced dopamine neurons (iDANs). Reprogramming efficiency *in vitro* is improved by small molecules that promote chromatin remodeling and activate the TGFβ, Shh and Wnt signaling pathways. The reprogramming efficiency of human astrocytes reaches up to 16%, resulting in iDANs with appropriate midbrain markers and excitability. In a mouse model of Parkinson's disease, NeAL218 alone reprograms adult striatal astrocytes into iDANs that are excitable and correct some aspects of motor behavior *in vivo*, including gait impairments. With further optimization, this approach may enable clinical therapies for Parkinson's disease by delivery of genes rather than cells.**

Parkinson's disease is a neurodegenerative disorder characterized by the progressive loss of midbrain dopamine neurons (mDAs) in the *substantia nigra*. Current treatments for the disease focus on symptomatic management through restoration of dopaminergic activity[1] but do not alter the progressive neurodegeneration. There is therefore a clear medical need for disease-modifying therapies. Cell replacement therapy has been proposed as one such approach. Initial efforts were based on the use of fetal midbrain tissue as a source of mDAs for transplantation[2,3]. However, difficulties in obtaining and standardizing fetal tissue led to the search for alternative cell sources, such as stem cells or reprogrammed cells[4,5]. Following the discovery that somatic cells can be reprogrammed into induced pluripotent stem (iPS) cells[6], we and others showed that rodent and human terminally differentiated somatic cells of meso-, endo- and ectodermal origin can be directly reprogrammed into different somatic cells, such as induced neurons (iNs)[7–9]. Moreover, both rodent and human fibroblasts have been reprogrammed into iDANs[10–13] capable of bringing some functional recovery after transplantation to animal models of Parkinson's disease[11,12].

More recently, direct *in vivo* reprogramming of adult glial cells has emerged as a possible approach for cell replacement therapy that would avoid the use of cell transplantation and immunosuppression. To date, iDANs have been generated only from mouse astrocytes *in vitro*[14]. *In vivo*, mouse glial cells have been reprogrammed to different types of neurons[5,15–23], but not iDANs[22].

Here we undertake the first two steps toward the development of direct *in vivo* reprogramming as a therapeutic approach for Parkinson's disease. First, we demonstrate reprogramming of human astrocytes into excitable iDANs *in vitro*. This is achieved using the NeAl218 cocktail and is further improved by treatment with small molecules. Second, we show direct *in vivo* reprogramming of adult striatal mouse astrocytes into functional iDANs, leading to rescue of spontaneous motor behavior, such as gait alterations, and correction of some aspects of drug-induced motor behavior in a unilateral 6-hydroxydopamine (6-OHDA) mouse model of Parkinson's disease. Our findings widen the spectrum of demonstrated cell fate switches of human somatic cells and suggest that direct *in vivo* astrocyte reprogramming is a viable potential strategy to restore motor function in Parkinson's disease.

## RESULTS

### Reprogramming immortalized human astrocytes into iDANs

In a first attempt to reprogram human astrocytes into iDANs, we infected a human immortalized astrocyte cell line of fetal origin (hIAs) with different lentiviruses carrying the reverse tet-transactivator (rtTA[24]) and genes encoding three transcription factors previously found to reprogram fibroblasts into iDANs[10]: ASCL1, LMX1A and NR4A2 (the latter also known as NURR1, collectively referred to as "ALN"). hIAs were cultured in Eagle's Minimum Essential Medium (EMEM) for 5 d and subsequently treated with doxycycline for 10 d to trigger transgene expression (basic protocol, BP; **Fig. 1a**). We first

[1]Laboratory of Molecular Neurobiology, Department of Medical Biochemistry and Biophysics, Karolinska Institutet, Stockholm, Sweden. [2]Department of Molecular Neurosciences, Center for Brain Research, Medical University of Vienna, Vienna, Austria. [3]Department of Neuroscience, Karolinska Institutet, Stockholm, Sweden. [4]Department of Pharmacology, Faculty of Medicine, Biomedical Research Institute of Malaga (IBIMA), Malaga University, Malaga, Spain. [5]Institute for Stem Cell Biology and Regenerative Medicine, Stanford University, Stanford, California, USA. Correspondence should be addressed to E.A. (ernest.arenas@ki.se).

Received 15 July 2016; accepted 22 February 2017; published online 10 April 2017; doi:10.1038/nbt.3835

confirmed that hIAs do not give rise to neurons in the absence of ALN, indicating that they are neither stem- nor neurogenic radial glia-like cells (**Supplementary Fig. 1a**). ALN infection gave rise to a small proportion (1.26 ± 0.4%) of tyrosine hydroxylase-positive ($TH^+$) cells at day 15 (**Fig. 1c**,**d**). However, these cells lacked both neuronal morphology and excitability. This conversion efficiency was considerably lower than the 6 ± 2% obtained previously after infection of human IMR90 fibroblasts with ALN under similar culturing conditions[10], reflecting cell type differences in reprogramming.

The conversion rate of hIAs into iDANs was improved by incorporating additional signals driving midbrain development (midbrain protocol, MP; **Fig. 1b**). hIAs were infected with ALN and treated for 7 d with the chromatin remodeling co-factor ascorbic acid[25], and the TGFβ and BMP4 inhibitors SB431542 and LDN193189, to improve neural induction[26]. Additionally, 2 d after the start of doxycycline treatment, the medium was changed to KON3, a version of the N3 medium[27]. Midbrain floorplate identity was induced with sonic hedgehog (SHH) and the GSK3β inhibitor CT99021 (ref. 28). This protocol sharply increased the number of $TH^+$ cells (17.5 ± 4.5%) and induced neuronal morphology as well as co-expression of the early neuronal marker β-III-tubulin (TUBB3), but not microtubule-associated protein 2 (MAP2), marking mature somatodendric axes (**Fig. 1c**,**d**). Notably, infection of hIA cells with a control virus harboring GFP or omission of the ALN transcription factors did not produce $TH^+$ or $TH^+$/$TUBB3^+$ cells (**Supplementary Fig. 1b**), indicating that viral transduction had no effect *per se* and that ALN was necessary for the generation of iDANs.

## NeAL218 is more efficient than ALN to reprogram human astrocytes into iDANs

We next examined the individual contributions of the ALN transcription factors in determining reprogramming efficiency. We found that AL was more efficient than ALN and A was more efficient than AN, indicating that NR4A2 limited the reprogramming of hIA cells into iDANs (**Fig. 1e**). We then investigated whether the conversion efficiency could be further increased by the incorporation of additional factors such as NEUROD1, which improves neural reprogramming of human cells[29], and miR218, which regulates mDA development[30]. We found that NeAL218 induced more iDANs than ALN (30.97 ± 5.3% vs. 17.5 ± 4.5%, respectively) followed by AL218 and AL (24.7 ± 6.5% and 24.3 ± 5.3%, respectively; **Fig. 1e**). In addition, NeAL218 also increased the number of mature $MAP2^+$ iDANs to up to 84.6 ± 1.9% (**Fig. 1f**). Moreover, the inclusion of miR218 and NEUROD1 in the reprogramming cocktail increased the expression of typical mDA genes such as *SLC6A3* (*DAT*), *FOXA2*, *EN1* and *SLC18A2* (*VMAT2*) by 5- to 20-fold (**Supplementary Fig. 1c**). NeAL218-MP-treated hIAs stained positively for TH, TUBB3 and MAP2, as well as the dopaminergic markers dopamine transporter (SLC6A3) and DOPA-decarboxylase (DDC; **Fig. 1g**). However, these cells exhibited simple neuron-like morphologies and lacked membrane properties of excitable mDAs.

## Increased iDAN reprogramming quality by chromatin remodeling agents and TGFβ

It has been reported that chromatin remodeling agents such as valproic acid[31] (VPA), 5-aza-2′-deoxycytidine[32] (Dec) and ascorbic acid[33] can improve the efficiency of somatic cell reprogramming. It has also been reported that the sequential induction of epithelial-mesenchymal transition and mesenchymal-epithelial transition increases the efficiency of iPS cell generation[34]. We examined whether a short TGFβ1 pulse, followed by overnight treatment with chromatin remodeling agents (VPA and Dec), and treatment with dual-Smad inhibitors (SB431542 and LDN193189) as well as

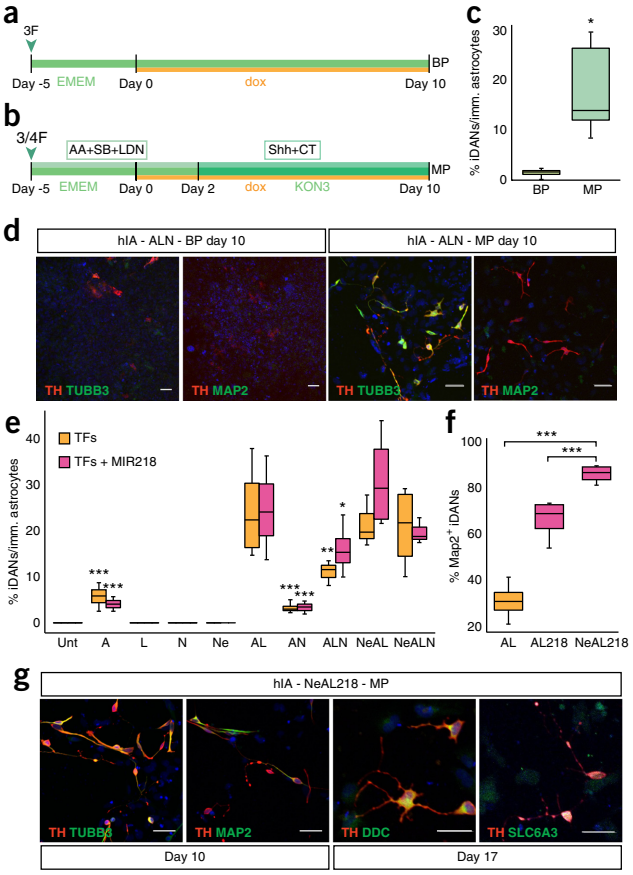


**Figure 1** Human astrocytes can be reprogrammed with NeAL218. (**a**,**b**) iDAN reprogramming was done with a basic protocol (BP) (**a**) or a midbrain protocol (MP) (**b**). (**c**) Quantification of the percentage of human immortalized astrocytes (hIA) that became $TH^+$ after infection with ALN after 10 d of doxycycline (dox) induction in BP or MP media. BP $n = 4$; MP $n = 5$. Two-tailed Student's *t*-test with unequal sample variance $P = 0.016$. (**d**) hIAs treated with ALN-MP, but not ALN-BP, showed presence of immature $TH^+$;$TUBB3^+$ neurons at day 10. (**e**) Quantification of the percentage of iDANs obtained with different combinations of transcription factors in MP medium at day 10. Untreated, miR218, A218, L, L218, N, N218, Ne, Ne218, AL218, AN218, ALN, NeAL and NeALN218, $n = 3$; A, AL, AN, ALN218, NeAL218 and NeALN, $n = 4$. One-way ANOVA followed by Dunnett's *post-hoc* multiple comparison test against the NeAL218 condition: A, $P = 0.0001$. NeAL218 vs. AN, $P = 0.0001$; NeAL218 vs. ALN, $P = 0.0059$; NeAL218 vs. A218, $P = 0.0002$. NeAL218 vs. AN218, $P = 0.0001$; NeAL218 vs. ALN218, $P = 0.0347$. (**f**) Quantification of the percentage of mature $MAP2^+$ iDANs obtained with AL-, AL218- or NeAL218-MP (for **e** and **f** multiple comparison test against the NeAl218 condition). AL, AL218 and NeAL218, $n = 4$. One-way ANOVA followed by Dunnett's *post-hoc* multiple comparison test against the NeAL218 condition: AL, $P = 0.0002$. NeAL218 vs. AL218, $P = 0.0001$. (**g**) $TH^+$ cells in NeAL218-MP cultures were also $TUBB3^+$, $MAP2^+$, $DDC^+$ and $SLC6A3^+$. Replicates are counts in independent experiments performed in duplicate. Data are expressed as box plots showing the median as well as the 25th and 75th percentiles. Scale bars, 50 μm. $^*P < 0.05$, $^{**}P < 0.001$ and $^{***}P < 0.0001$.

midbrain patterning signals (CT99021 and purmorphamine) could improve the reprogramming efficiency of astrocytes into iDANs. The efficacy of this 'remodeling TGFβ midbrain protocol' (RTMP, **Fig. 2a**) on reprogramming was compared to the previous MP protocol after 13 d of doxycycline induction (**Fig. 1b**). While the number of $TH^+$ cells was lower with RTMP than with the MP protocol (16.48 ± 8.6% vs. 30.97 ± 5.3%, respectively), the quality of iDAN

reprogramming improved, as shown by the presence of MAP2, SYN1 (Synapsin), DDC, SLC6A3, KCNJ6 (GIRK2) and ALDH1A1 in TH$^+$ cells (**Fig. 2b**). Notably, the number of TH$^+$ cells did not vary between days 4 and 10 in the NeAL218-RTMP protocol (**Supplementary Fig. 2a**), but their maturation improved over time (**Supplementary Fig. 2b**).

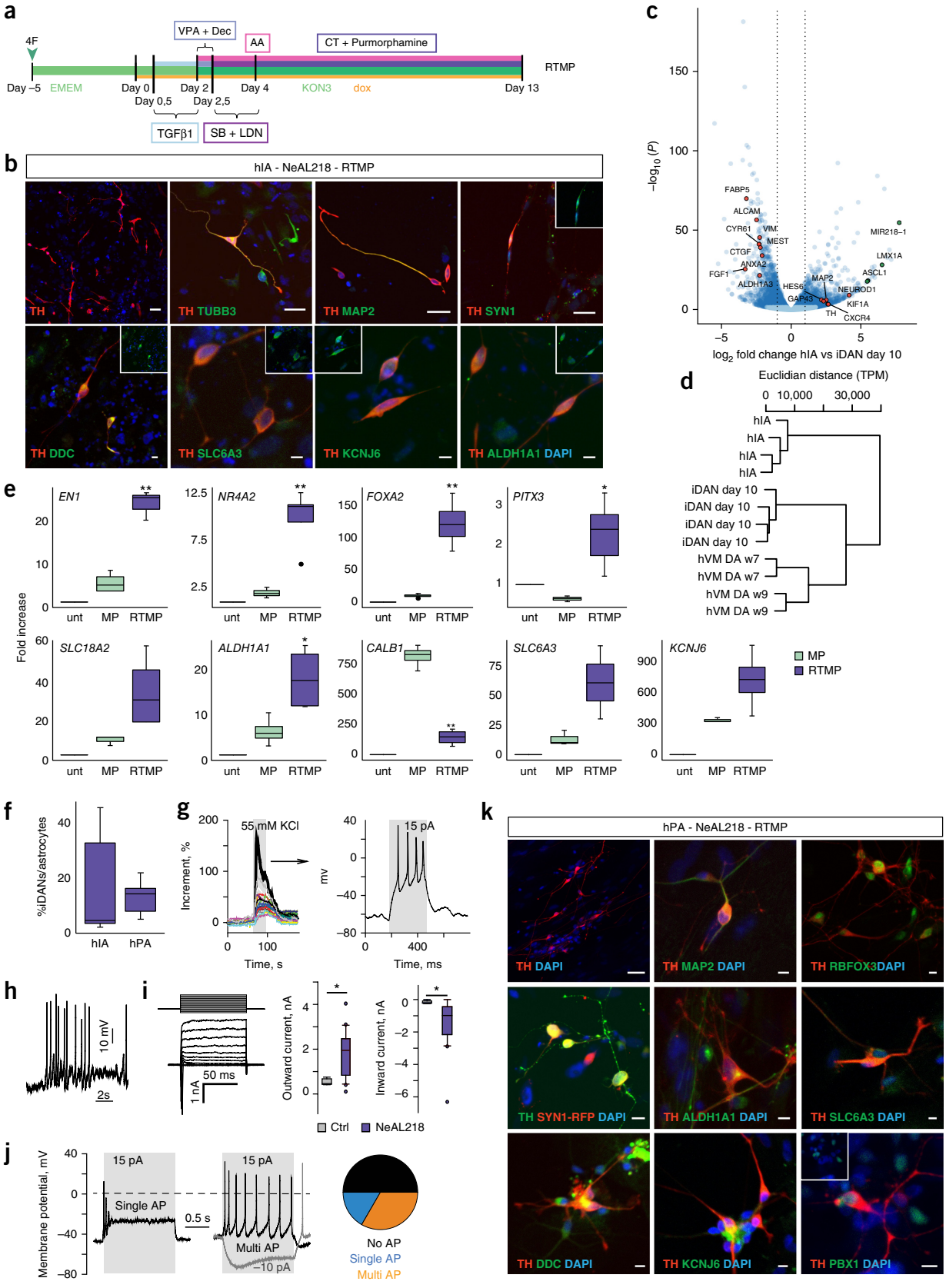

**Table 1 Summary of the stepwise improvements in the iDAN reprogramming protocol**

| Input | | | Output | | | |
|---|---|---|---|---|---|---|
| Cells | Lentiviruses | Protocol | Readout | | | |
| Human astrocytes | Reprogramming factors | Media | %iDANs | Morphology | IHC | Action potentials |
| Immortalized | ALN | BP | 1.26 (±0.4) | Astrocytic | TH | None |
| Immortalized | ALN | MP | 17.5 (±4.5) | Neuronal | TH, TUBB3 | None |
| Immortalized | NeAL218 | MP | 30.97 (±5.3) | Neuronal | TH, TUBB3, MAP2, DDC, SLC6A3 | None |
| Immortalized | NeAL218 | RTMP | 16.48 (±8.6) | Neuronal | TH, TUBB3, MAP2, DDC, SLC6A3, KCNJ6, ALDH1A1, SYN1 | Single |
| Primary | NeAL218 | RTMP | 12.4 (±2.7) | Neuronal | TH, MAP2, DDC, SLC6A3, SYN1, KCNJ6, ALDH1A1, RBFOX3, PBX1 | Multiple |

IHC, immunohistochemistry.

In order to characterize the transcriptome of iDANs, we compared genes differentially expressed in hIAs at -5 d and iDANs$^{NeAL218\text{-}RTMP}$ at 10 d of doxycycline induction to the dopaminergic signature of human embryonic midbrain (gestational weeks 7 and 9; ref. 35). We found that our reprogramming protocol reduced the expression of glial genes, such as *FABP5*, *ALCAM*, *VIM*, *CYR61*, *CTGF*, *MEST*, *ANXA2*, *FGF1* and *ALDH1A3* (ref. 35), while inducing the expression of genes involved in the switch between glia and neurons, such as *HES6* (refs. 36,37), and of genes involved in neuronal differentiation (*MAP2*, *GAP43*, *KIF1A*) and expressed in mDA neurons (*CXCR4*, *TH*; **Fig. 2c**). As a result, the transcriptomic profiles of iDANs$^{NeAL218\text{-}RTMP}$ were closer to those of endogenous human mDA neurons than to those of hIAs (**Fig. 2d**). Moreover, real-time qPCR confirmed the expression of midbrain-specific transcription factors (*EN1*, *NR4A2*, *FOXA2* and *PITX3*) in cells treated with the NeAL218-RTMP protocol, but not with the NeAL218-MP protocol, or in untreated hIAs (**Fig. 2e**). Furthermore, the expression of genes typical of mDA neurons (*SLC6A3*, *SLC18A2*) and predominantly expressed in *substantia nigra* neurons, as *KCNJ6* and *ALDH1A1*, increased, while the expression of *CALB1*, a marker of ventral tegmental area neurons, decreased (**Fig. 2e**). We also detected mature TH$^+$;MAP2$^+$ neurons with long processes, similar to iDANs reprogrammed from fibroblasts[10,13], and the presence of TH$^+$;SYN1$^+$ structures, as well as TH$^+$;DDC$^+$, TH$^+$;SLC6A3$^+$, TH$^+$;KCNJ6$^+$ and TH$^+$;ALDH1A1$^+$ cells (**Fig. 2b**). These results suggest that the combination of transcription factors and small molecules in the NeAL218-RTMP protocol efficiently increased the acquisition of midbrain regional identity in hIA-derived iDANs. In addition, reprogramming of hIAs into iDANs$^{NeAL218\text{-}RTMP}$ was stable, as removal of doxycycline by day 7 or 10 (**Supplementary Fig. 2c**) did not change marker expression, cell morphology or survival at day 13 (**Supplementary Fig. 2d**). Finally, analysis of the electrophysiological properties of hIA-derived iDANs$^{NeAL218\text{-}RTMP}$ revealed that only a few cells were able to generate single action potentials, even though they had voltage-gated inward and outward currents (**Supplementary Fig. 2e–i**).

## Enhanced iDAN functionality by reprogramming of primary human astrocytes

Considering that the capacity of hIA to differentiate into excitable mature neurons may be impaired by their immortalization with SV40 (ref. 38), we examined whether human primary embryonic astrocytes (hPAs) could be reprogrammed into mature functional iDANs. While no spontaneous differentiation was observed when we treated hPAs with the RTMP protocol alone (**Supplementary Fig. 3a–c**), we reprogrammed NeAL218-RTMP primary astrocytes into TH$^+$ cells with an efficiency of 12.4 ± 2.7% (**Fig. 2f**).

hPA cells exposed to the NeAL218-RTMP protocol expressed not only mature neuronal markers (MAP2, RBFOX3 (also known as NEUN) and SYN1) in TH$^+$ cells but also appropriate mDA markers, including KCNJ6, SLC6A3, DDC, ALDH1A1 and PBX1 (**Fig. 2k** and **Supplementary Fig. 3d**). Moreover, calcium imaging revealed the presence of cells responding to depolarizing stimuli with multiple action potentials (**Fig. 2g**). A more detailed analysis of membrane properties by patch-clamp electrophysiology identified cells with rapid autonomous spiking activity (**Fig. 2h**), inward and outward voltage-gated currents (**Fig. 2i**), capacity to generate multiple and broad (1.9 ± 0.2 ms) action potentials in 33% of all rRecorded cells on day 14 *in vitro*, as well as the presence of delayed voltage rectification (sag) typical of mDA neurons (**Fig. 2j**). These results indicate that primary human astrocytes can be reprogrammed into functionally competent iDANs by NeAL218-RTMP *in vitro* (**Table 1**).

**Figure 2** Small molecules increase maturation of human-astrocyte-derived iDANs. (**a**) Remodelling TGFβ Midbrain Protocol (RTMP). (**b**) Confocal images of TH$^+$ iDANs, which were TH$^+$ iDANs were also TUBB3$^+$, MAP2$^+$, SYN1$^+$, DDC$^+$, SLC6A3$^+$, KCNJ6$^+$ and ALDH1A1$^+$ after 13–17 d. Scale bars: upper row, 50 µm; lower row, 10 µm. (**c**) Comparison of the transcriptional profiles of hIAs and iDANs$^{NeAL218\text{-}RTMP}$ at day 10. Selected genes are shown over the threshold (0.05) and above twofold change of expression (dotted lines). Green circles, the reprogramming factors; red circles, selected neuronal and astrocytic genes. (**d**) Hierarchical clustering of transcriptome expression of hIAs, iDANs$^{NeAL218\text{-}RTMP}$ at day 10, and the dopaminergic signature of the human embryonic VM. Scale: Euclidian distance. TPM, transcripts per million. (**e**) Gene expression analysis by real-time qPCR data of hIAs untreated or treated with NeAL218-MP or NeAL218-RTMP at day 10. *P* values for Student's *t*-test between MP and RTMP conditions: $*P < 0.05$, $**P < 0.01$. Two-tailed Student's *t*-test with unequal variance, MP vs. *RTMP*: *EN1* $P = 0.0039$; *NR4A2* $P = 0.0032$; *FOXA2* $P = 0.0095$; *PITX3* $P = 0.01$; *ALDH1A1* $P = 0.01$; *CALB1* $P = 0.00001$. (**f**) Quantification of the percentage of iDANs$^{NeAL218\text{-}RTMP}$ obtained from human immortalized (hIA) or primary (hPA) astrocytes. hIA and hPA, $n = 3$. (**g**) $Ca^{2+}$ responses in hPA-derived iDANs$^{NeAL218\text{-}RTMP}$: upon depolarization (55 mM KCl, left panel) and 15 pA current injection in the cell with the thickest trace, action potentials (AP) were generated (right panel). (**h**) Spontaneous electrical activity accompanied by generation of action potentials in hPA-derived iDANs$^{NeAL218\text{-}RTMP}$ at days 13–17. (**i**) Voltage-clamp recordings in hPA cells; left, representative current profiles of cells treated with NeAL218-RTMP; middle and right panels, quantification of amplitudes in NeAL218-RTMP-treated cells ($n = 21$) and control-RTMP cells ($n = 5$) for VG outward currents (at command voltage +50 mV, middle) and voltage-gated (VG) inward currents (in peak, right). $*P < 0.05$ and $**P < 0.001$. (**j**) Current-clamp recordings of NeAL218-RTMP-treated hPA cells reveal different firing properties upon current injections: silent cells (no AP), cell generating single AP on depolarization (left panel) and cells generating multiple AP (right panel), also demonstrating the recognizable voltage rectification (sag) in response to the neuron hyperpolarization (gray trace, 2 out of 7 neurons generating multiple AP). Pie chart shows the mean percentage of cells with AP ($n = 21$). (**k**) Confocal images showing that hPA-derived iDANs$^{NeAL218\text{-}RTMP}$ are immunoreactive to TH and MAP2, RBFOX3, SYN1, ALDH1A1, SLC6A3, DDC, KCNJ6 and PBX1 after 14 d. Scale bars: 10 µm, except for upper left image, 50 µm.

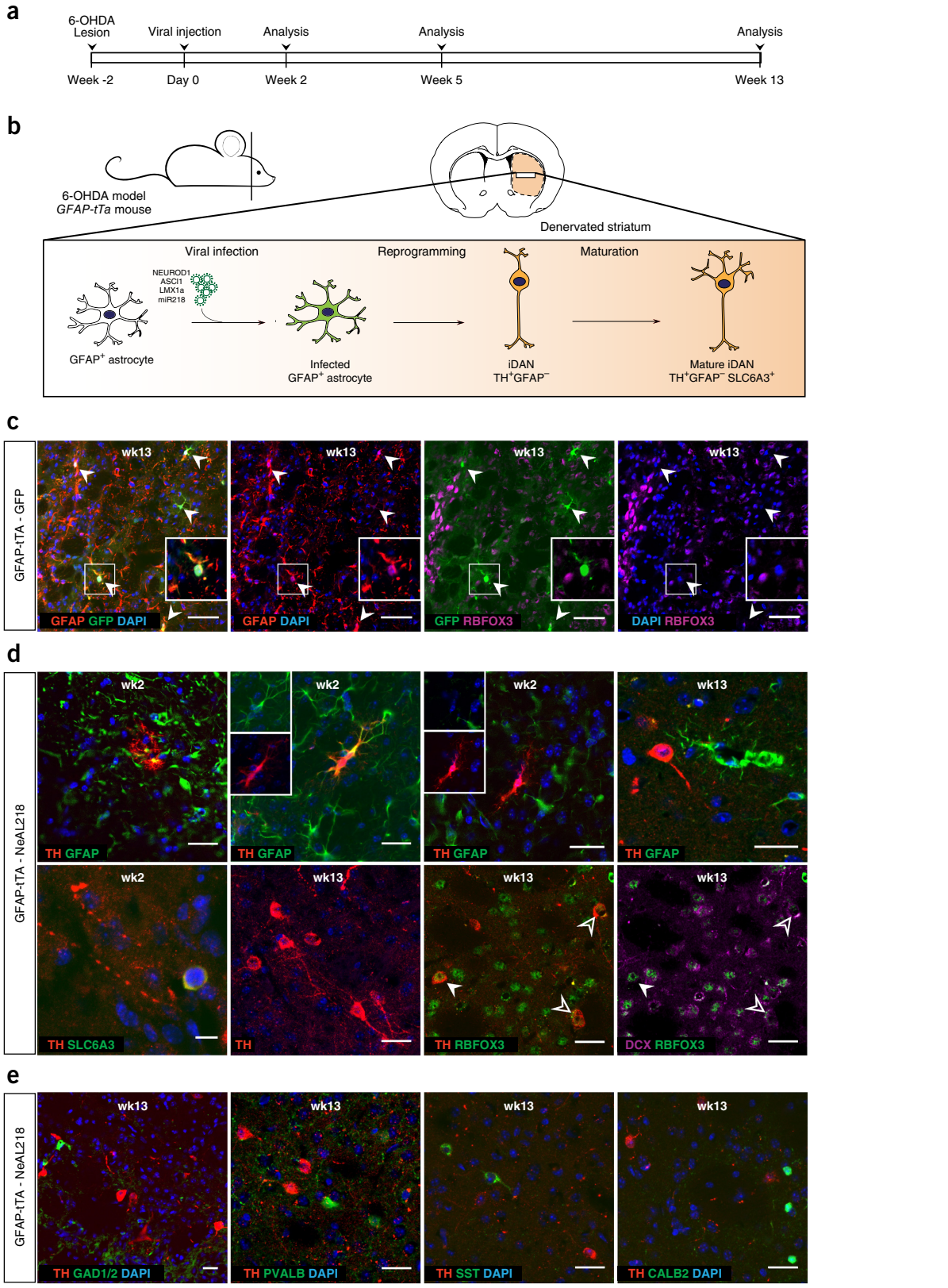


**Figure 3** NeAL218 reprograms astrocytes into iDANs *in vivo*. (**a**) Outline of the *in vivo* experiment. (**b**) Diagram depicting the reprogramming process *in vivo*. (**c**) Striata of *GFAP-tTA* adult mice infected with GFP 13 weeks after viral injection. White arrowhead, GFAP$^+$;GFP$^+$;RBFOX3$^-$ cell; insets show one cell at higher magnification. (**d**) iDANs in *GFAP-tTA* mice infected with NeAL218 show different degrees of reprogramming. Insets show examples of GFAP$^+$;TH$^+$;DAPI$^+$ and GFAP$^-$;TH$^+$;DAPI$^+$ cells. Solid arrowhead, TH$^+$;RBFOX3$^+$ cell; empty arrowhead, TH$^+$;DCX$^+$ cell. (**e**) TH$^+$ iDANs in *GFAP-tTA* mice infected with NeAL218 were negative for striatal neuron markers. Scale bars, 25 μm; for SLC6A3 in **d**, 10 μm. Wk, week.

### Direct *in vivo* conversion of mouse astrocytes into iDANs

Next, we investigated whether astrocytes can give rise to iDANs in a mouse model of Parkinson's disease. We used the NeAL218 factors alone, without RTMP medium, in adult mice unilaterally lesioned with 6-hydroxydopamine (6-OHDA[39]). This animal model of Parkinson's disease induces mDA neuron loss in the ipsilateral ventral midbrain (**Supplementary Fig. 4a**), as well as denervation and reactive gliosis in the striatum ipsilateral to the 6-OHDA lesion (**Supplementary Fig. 4b**). Two weeks after the 6-OHDA infusion, Tet-regulated NeAL218 or GFP lentiviruses were injected into the ipsilateral striatum of transgenic mice in which the tetracycline transactivator is under the control of the *gfap* promoter (*GFAP-tTA* mice, **Fig. 3a**,**b**). This genetic construct allows the expression of transgenes exclusively in astrocytes, in the absence of doxycycline, as shown by the exclusive presence of GFP in striatal GFAP$^+$;RBFOX3$^-$ cells at 2–13 weeks after GFP lentiviral delivery (**Fig. 3c** and **Supplementary Fig. 4c**). Notably, no partially reprogrammed GFP$^+$;TH$^+$ cells were detected at 13 weeks (**Supplementary Fig. 4d**), and none of the animals developed tumors or died during the course of the experiments.

Two weeks after NeAL218 injection, TH$^+$ cells were identified at different stages of reprogramming, including TH$^+$;GFAP$^+$ cells with mixed astrocyte-to-neuron morphology, as well as TH$^+$;GFAP$^-$ and TH$^+$;SLC6A3$^+$ cells with neuronal morphology (**Fig. 3d**). We also found that newly generated iDANs were either DCX$^+$ (doublecortin, a marker for early migratory neurons) or the mature neuronal marker RBFOX3$^+$, showing that they mature at variable rates into neurons (**Fig. 3d**). Notably, iDANs were abundant by 15 weeks after 6-OHDA injection (14.63 ± 8.5 TH$^+$ cells/section; seven sections/animal, $n = 7$), a finding that distinguishes iDANs from transient lesion-induced striatal neurons, which start decaying 1 week after lesion[40]. Moreover, iDANs, unlike lesion-induced striatal TH$^+$ neurons[41], did not express GAD1/2, somatostatin (SST), parvalbumin (PVALB) or calretinin (CALB2) (**Fig. 3e**), indicating that they do not derive from or acquire a striatal neuron phenotype.

### Characterization of the maturation and electrophysiological properties of iDANs generated *in vivo*

We next examined whether iDANs *in vivo* express the dopamine transporter, *Slc6a3*, which is present in mDA neurons but absent in TH$^+$ striatal neurons[40]. For this purpose we used the *GFAP-tTa;SLC6A3$^{Cre/+}$;Rosa26R$^{Tomato}$* reporter mice (**Fig. 4**, **Supplementary Fig. 4f**) or the *GFAP–tTa;SLC6A3$^{Cre/+}$* mice injected with intrastriatal flex-Tomato virus (**Supplementary Fig. 5a**). Analysis of 6-OHDA-lesioned SLC6A3 reporter mice injected with GFP into the striatum showed no



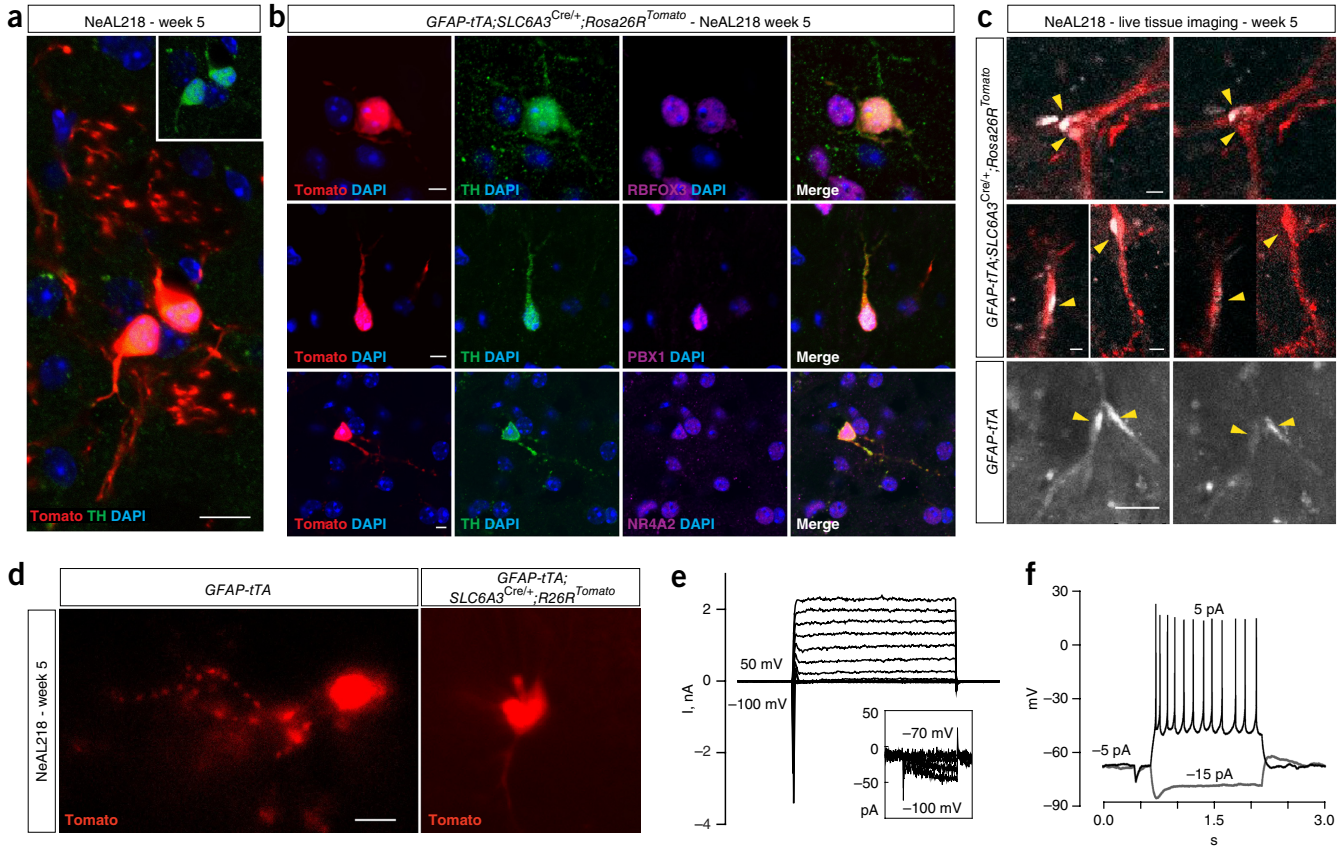


**Figure 4** Reprogramming of adult striatal astrocytes into functional iDANs by NeAL218 *in vivo*. (**a**,**b**) Micrographs of brain cryosections from SLC6A3$^{Tomato+}$ reporter mice intrastriatally injected with NeAL218 5 weeks after infection. (**a**) Presence of SLC6A3$^{Tomato+}$;TH$^+$ iDAN cell bodies and processes in the lesioned and injected striata. (**b**) SLC6A3$^{Tomato+}$;TH$^+$ iDANs in mice infected with NeAL218 showed positive staining for RBFOX3, NR4A2 and PBX1. (**c**) Time-lapse microphotographs showed KCl-induced release of FFN206, a fluorescent dopamine derivative, from SLC6A3$^{Tomato+}$;TH$^+$ iDANs in 250 µm-thick acute brain slices of *GFAP-tTa;SLC6A3$^{Cre/+}$;Rosa26R$^{Tomato}$* or from *GFAP-tTa;SLC6A3$^{Cre/+}$* adult mice 5 weeks after NeAL218 injection. (**d**) Examples of patch-recorded SLC6A3$^{Tomato+}$-reprogrammed iDANs patched 5 weeks after viral infection, in 250 µm-thick acute brain slices. (**e**) Voltage-gated currents at incrementing polarization steps lasting 100 ms. Inset: hyperpolarization-activated currents in voltage-clamp recordings upon hyperpolarization steps to –90 and –100 mV. (**f**) Current-clamp trace showing the ability of iDANs to generate repetitive action potentials (black) and their voltage sag rectification upon somatic current injection (gray). Scale bars in **a**: 10 µm; **b**–**d**: 5 µm.

SLC6A3$^{Tomato+}$;TH$^{+}$ cells (**Supplementary Fig. 4e**), while NeAL218 injection revealed the presence of SLC6A3-driven Tomato$^{+}$ cells that were identified as TH$^{+}$ iDANs, exhibiting a mature neuronal morphology (**Fig. 4a**). These cells also expressed the mature neuronal marker RBFOX3 and transcription factors typical for mDA neurons such as NR4A2 and PBX1 (**Fig. 4b**). At a functional level, in acute striatal slices from 6-OHDA-lesioned mice injected with NeAl218, we found that several SLC6A3$^{Tomato+}$cells were able to

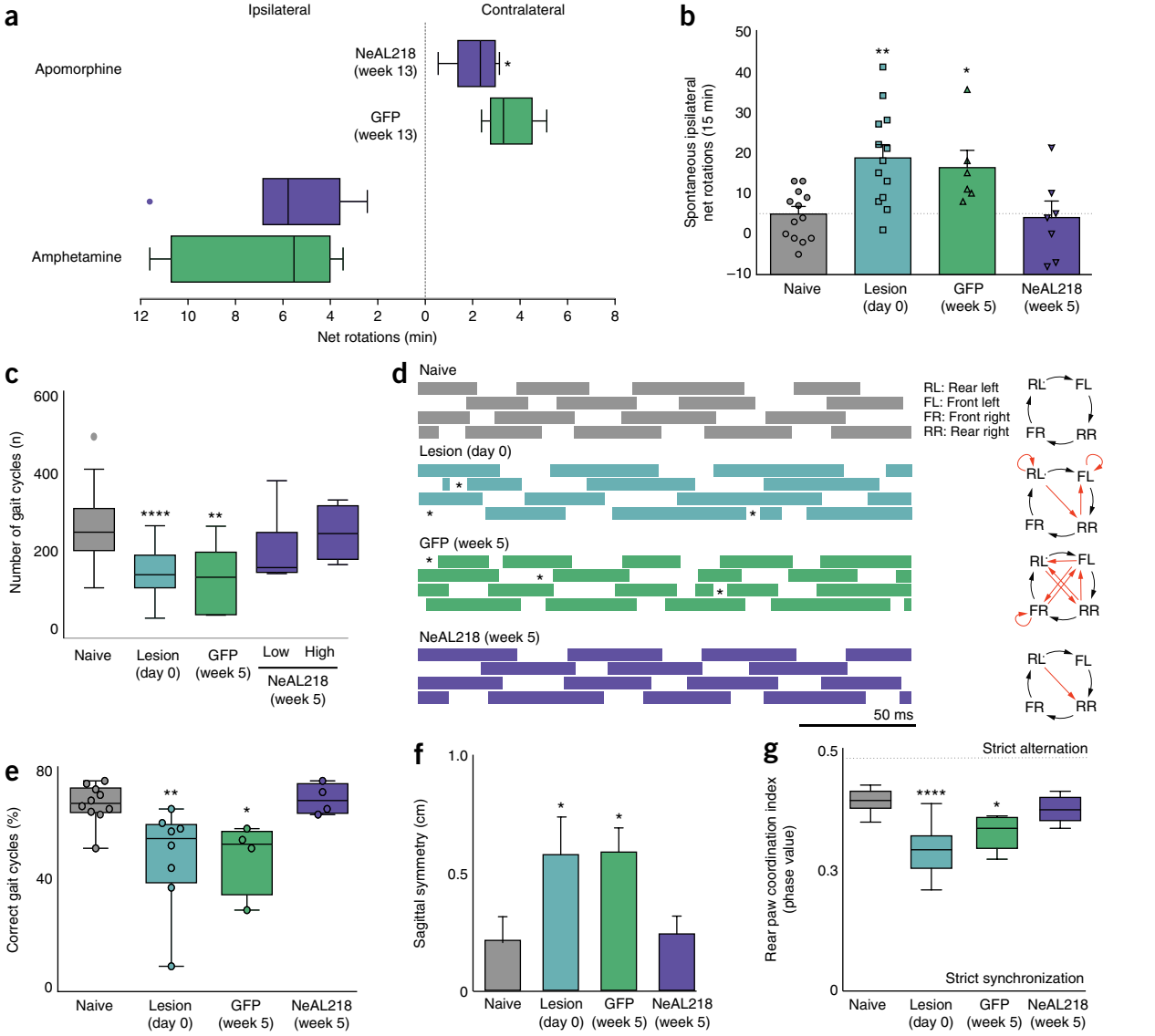


**Figure 5** iDANs$^{NeAL218}$ induce behavioral recovery in a mouse model of Parkinson's disease. (**a**) Net rotations (expressed as rotations/min) induced by amphetamine or apomorphine 13 weeks after NeAL218 or GFP injection (GFP $n = 6$, NeAL218 $n = 7$). Tukey whiskers plot with the median, 10th, 25th, 70th and 90th percentiles. Mann–Whitney rank sum test for apomorphine $P = 0.035$ and for amphetamine $P = 0.917$ (two tailed). (**b**) Spontaneous ipsilateral rotations (expressed as rotations/15 min) 5 weeks after NeAL218 or GFP injection (naive $n = 13$, lesion $n = 13$, GFP $n = 6$, NeAL218 $n = 7$). One-way ANOVA, $F_{(3,35)} = 6.03$; $P = 0.002$ followed by Holm–Sidak's comparison; lesion vs. naive $P = 0.003$; GFP vs. naive $P = 0.0493$ and NeAL218 vs. naive $P = 0.843$. (**c**–**g**) Gait analysis showing: (**c**) total number of gait cycles (naive $n = 24$, lesion $n = 22$, GFP $n = 11$, NeAL218 low dose $n = 7$, NeAL218 high dose $n = 4$). Tukey whiskers plot. Kruskal–Wallis test $P < 0.0001$ followed by Dunn's comparison; lesion vs. naive $P < 0.0001$; GFP vs. naive $P = 0.0012$; NeAL218 low vs. naive $P = 0.3622$ and NeAL218 high vs. naive $P > 0.999$. (**d**) Right, examples of consecutive step cycle for all limbs during walk (naive $n$ =10, 6-OHDA-lesion $n = 8$, lesion-GFP $n = 4$ and lesion-NeAL218 mice $n = 4$). Gait was examined using ventral plane videography system. The horizontal bars represent the time during which a paw makes contact with the floor (direction of travel left to right). Asterisks mark hesitations in the gait cycle. (**d**) Left, diagrams depicting the movement order of the limbs during gait cycles. Black arrows indicate correct ordering of paw-treadmill-contacts. Red arrows highlight step cycle deviations. (**e**) Percentage of correct paw ordering cycles; box and whiskers graph showing min to max and all individual data. One-way ANOVA, $F_{(3,22)} = 5.42$; $P = 0.006$ followed by Dunnett's comparison; lesion vs. naive $P = 0.009$; GFP vs. naive $P = 0.0435$; NeAL218 vs. naive $P = 0.991$. (**f**) Sagittal gait symmetry (zero: bilaterally symmetric gait). Bar graphs, mean ± s.e.m. Data were analyzed with one sample $t$-test with theoretical mean equal to 0 (two-tailed). Naive $P = 0.383$; lesion $P = 0.0218$; GFP $P = 0.0231$ and NeAL218 $P = 0.178$; and (**g**) coordination index (phase value) representing rear limbs synchronicity in naive $n$ =10, 6-OHDA-lesion $n = 8$, lesion-GFP $n = 4$ and lesion-NeAL218 mice $n = 4$. Tukey whiskers plot, no outlier found. Kruskal–Wallis test $P < 0.0001$ followed by Dunn's comparison; lesion vs. naive $P < 0.0001$; GFP vs. naive $P = 0.0193$; NeAL218 vs. naive $P > 0.999$. *$P < 0.05$; **$P < 0.01$; ***$P < 0.001$; ****$P < 0.0001$.

take up fluorescent dopamine (FFN206) and release it upon KCl-induced depolarization (**Fig. 4c** and **Supplementary Fig. 5b**), suggesting the presence of active SLC18A2 and SLC6A3 (refs. 42,43) n iDANs. Fluorescence-mediated cell identification also allowed for patch-clamp recordings in striatal slices *ex vivo*, 5 weeks after viral injection. Electrophysiological recordings revealed the capacity of iDANs to reliably generate action potentials (**Fig. 4d–f**). We analyzed data from 28 NeAL218-induced SLC6A3$^{Tomato+}$ cells and found that 9 of them were capable of producing action potentials, including action potential trains in 5 of them, with an average maximum frequency approaching 15 Hz (**Fig. 4e**,**f** and **Supplementary Fig. 5c–e**). Together, these experiments revealed the presence of excitable iDANs expressing midbrain markers, such as SLC6A3-driven Tomato, NR4A2 and PBX1. Moreover, NeAL218-derived SLC6A3$^{Tomato+}$ cells presented hyperpolarization-activated currents ($I_h$) in voltage-clamp recordings upon hyperpolarization steps to −90 and −100 mV, (**Fig. 4e**, insert), causing delayed voltage rectification (or sag; **Fig. 4f**, hyperpolarization trace), which is considered a biophysical signature of mDA neurons. In contrast, GFP$^+$ cells in animals injected with a GFP lentivirus alone lacked excitability and the capacity to generate action potentials (**Supplementary Fig. 5f**). These results show that iDANs are excitable and exhibit properties of mDA neurons.

### iDANs rescue spontaneous motor behavior in a 6-OHDA model of Parkinson's disease

We then examined whether iDANs could induce motor recovery in *GFAP-tTa* mice with ipsilateral 6-OHDA lesions, as assessed by drug-induced and spontaneous motor activity.

Drug-induced circling behavior has been traditionally used in combination with unilateral lesion models to examine the functionality of mDA neurons[44]. Rotations induced by apomorphine decreased in animals treated with NeAL218, compared to GFP, 13 weeks after viral injection (**Fig. 5a**). This result indicated that iDANs promoted DA transmission in the DA-depleted striatum, thereby reducing the development of DA receptor sensitization in striatal target neurons, which is the basis of the apomorphine-induced circling behavior[45]. However, there was no effect on rotations induced by amphetamine (**Fig. 5a**, **Supplementary Fig. 5g**), a behavior generated by inhibiting or reversing DA transport by SLC6A3, which leads to an abnormal concentration of DA in synapses. Nonetheless, spontaneous circling behavior, which emerges as a consequence of the severe unilateral loss of striatal DA, was completely rescued by NeAL218, but not by GFP, 5 weeks after viral injection in mice unilaterally injected with 6-OHDA (**Fig. 5b**). These results suggest that iDANs$^{NeAL218}$ do not release the very high levels of DA that are required in the synapses to induce circling behavior in response to amphetamine, but are capable of correcting basal and postsynaptic deficits in DA transmission.

We then performed a more detailed analysis of spontaneous motor behavior and examined coordinated limb usage during voluntary locomotion, a function that is impaired and relevant for Parkinson's disease patients[46]. Computer-based analysis of spontaneous gait cycles on a treadmill[47,48] revealed a pronounced decline in motor performance induced by 6-OHDA, resulting in incomplete gait cycles (**Fig. 5c**). While injection of GFP lentivirus did not improve gait in lesioned mice, injection of NeAL218 restored the number of complete gait cycles 5 weeks after viral injection in a dose-dependent manner (**Fig. 5c**), indicating that the effects of NeAL218 are specific. 6-OHDA lesioned mice also showed sequence irregularities in limb usage resulting in movement fragmentation (**Fig. 5d**) and reduced the percentage of gate cycles with correct paw usage (**Fig. 5e**). These behaviors were not modified by GFP lentiviral injection but were rescued by NeAL218 to a level similar to that of naive mice. Similarly, axial symmetry and gait, two parameters typically altered in Parkinson's disease patients[46] and Parkinson's disease mouse models[49], were restored in NeAl218-injected mice, allowing performances similar to that of naive animals (**Fig. 5f**,**g**). These results demonstrate that direct *in vivo* reprogramming of astrocytes into iDANs counteracted deficits in spontaneous motor function in experimental Parkinsonism that are relevant to the disease.

## DISCUSSION

Previous studies have shown that rodent astrocytes can be reprogrammed into induced neurons[5,15–23], but a dopaminergic phenotype has not yet been obtained from either human astrocytes *in vitro* or mouse striatal astrocytes *in vivo*. Here we provide evidence of the capacity of human astroglia to be reprogrammed into iDANs capable of expressing sets of midbrain-specific transcription factors and typical dopaminergic markers, adopting mature neuronal morphology and functionality. Unlike other reprogramming protocols[50], we found that the ability of NeAL218 to convert astrocytes into iDANs is conserved from mouse to human and from *in vitro* to *in vivo*. The efficiency of human astrocyte reprogramming, as well as the acquisition of midbrain markers, sharply increased by sequential treatment with growth factors (TGFβ1) and small molecules (VPA, Dec, SB, LDN, AA, CT and purmorphamine) that promote chromatin remodeling and mimic midbrain development. These findings indicate that human astrocytes are not only amenable to reprogramming but also capable of adequately responding to developmental cues.

A previous study found that intrastriatal delivery of ALN via adeno-associated viruses did not reprogram oligodendrocyte precursors or astrocytes into iDANs in NG2-or GFAP-Cre mice that did not receive a dopaminergic lesion[22]. In our study, *GFAP-tTA* mice received 6-OHDA injections to mimic the loss of mDA neurons and the reactive gliosis found in Parkinson's disease[51]. The latter may be of particular importance as reactive gliosis is known to increase the number of reprogrammable astrocytes[20]. Moreover, our results show that ALN is less efficient than NeAL218 at reprogramming astrocytes into iDANs *in vitro* and that a very high titer of NeAL218 lentivirus is required for efficient iDAN generation in 6-OHDA lesioned *GFAP-tTA* mice.

Our finding that adult mouse striatal astrocytes can be reprogrammed *in situ* into functional iDANs that rescue some aspects of motor behavior in an animal model of Parkinson's disease supports future development of this strategy as a treatment for the disease. The next steps to be taken toward achieving this goal include improving reprogramming efficiency, demonstrating the approach on human adult striatal astrocytes, developing systems to selectively target human striatal astrocytes *in vivo*, and ensuring safety and efficacy in humans.

## METHODS

Methods, including statements of data availability and any associated accession codes and references, are available in the online version of the paper.

*Note: Any Supplementary Information and Source Data files are available in the online version of the paper.*

ACKNOWLEDGMENTS

We thank the members of the Arenas laboratory for help and suggestions; J. Söderlund and A. Nanni for technical and secretarial assistance; and the SciLife National Genomic Infrastructure (Stockholm) for RNA sequencing. This work was supported by grants from the Swedish Research Council (VR: DBRM, 2011-3116/3318 and 2016-01526), Swedish Foundation for Strategic Research (SRL), EU (NeuroStemcellRepair and DDPDgenes), Karolinska Institutet, Strat Regen, Hjärnfonden (FO2013:0108, FO2015:0202) and Cancerfonden (CAN 2016/572)

to E.A.; VR (2012-13482 and 2015-02886), StratNeuro, Parkinsonfonden, Hjärnfonden and KI/NIH to G.F.; VR (2013-3080), EU (PAINCAGE), Hjärnfonden, NovoNordisk Foundation and the European Research Council ("Secret Cells") to T.H.; and New York Stem Cell Foundation, NIH and CIRM to M.W. Support to P.R.d.V.C. was provided by VR (524-2011-962) and EMBO (ALTF583-2011); to R.A.R. by EMBO (ALTF596-2014) and Marie Curie (EMBOCOFUND2012, GA-2012-600394); to D.M. by KI and by the Brasilian Ministry of Education (CAPES) and to E.M.-M. by the Spanish Ministry of Education (José Castillejo). The authors acknowledge support from Science for Life Laboratory, the Knut and Alice Wallenberg Foundation, the National Genomics Infrastructure funded by the Swedish Research Council, and Uppsala Multidisciplinary Center for Advanced Computational Science for assistance with massively parallel sequencing and access to the UPPMAX computational infrastructure.

## AUTHOR CONTRIBUTIONS

E.A. and P.R.d.V.C. conceived the experiments and wrote the manuscript; P.R.d.V.C., R.A.R., G.S., D.M., E.M.-M., E.M.T., G.L.M., M.F., C.P., Y.-H.N. and S.P.S. performed the experiments; S. L., M.W., T.H., G.F. and E.A. provided expertise and funding.

## COMPETING FINANCIAL INTERESTS

The authors declare no competing financial interests.





1. DeMaagd, G. & Philip, A. Parkinson's disease and its management. Part 2: Introduction to the pharmacotherapy of parkinson's disease, with a focus on the use of dopaminergic agents. *P&T* **40**, 591–600 (2015).
2. Brundin, P. *et al.* Intracerebral grafting of dopamine neurons. Experimental basis for clinical trials in patients with Parkinson's disease. *Ann. NY Acad. Sci.* **495**, 473–496 (1987).
3. Lindvall, O. *et al.* Fetal dopamine-rich mesencephalic grafts in Parkinson's disease. *Lancet* **2**, 1483–1484 (1988).
4. Arenas, E. Towards stem cell replacement therapies for Parkinson's disease. *Biochem. Biophys. Res. Commun.* **396**, 152–156 (2010).
5. Arenas, E., Denham, M. & Villaescusa, J.C. How to make a midbrain dopaminergic neuron. *Development* **142**, 1918–1936 (2015).
6. Takahashi, K. & Yamanaka, S. Induction of pluripotent stem cells from mouse embryonic and adult fibroblast cultures by defined factors. *Cell* **126**, 663–676 (2006).
7. Vierbuchen, T. *et al.* Direct conversion of fibroblasts to functional neurons by defined factors. *Nature* **463**, 1035–1041 (2010).
8. Ladewig, J., Koch, P. & Brustle, O. Leveling Waddington: the emergence of direct reprogramming and the loss of cell fate hierarchies. *Nat. Rev. Mol. Cell Biol.* **14**, 225–236 (2013).
9. Chen, G. *et al.* In vivo reprogramming for brain and spinal cord repair(1,2,3). *eNeuro.* **2**, e0106–15.2015 (2015).
10. Caiazzo, M. *et al.* Direct generation of functional dopaminergic neurons from mouse and human fibroblasts. *Nature* **476**, 224–227 (2011).
11. Kim, J. *et al.* Functional integration of dopaminergic neurons directly converted from mouse fibroblasts. *Cell Stem Cell* **9**, 413–419 (2011).
12. Liu, X. *et al.* Direct reprogramming of human fibroblasts into dopaminergic neuron-like cells. *Cell Res.* **22**, 321–332 (2012).
13. Pfisterer, U. *et al.* Direct conversion of human fibroblasts to dopaminergic neurons. *Proc. Natl. Acad. Sci. USA* **108**, 10343–10348 (2011).
14. Addis, R.C. *et al.* Efficient conversion of astrocytes to functional midbrain dopaminergic neurons using a single polycistronic vector. *PLoS One* **6**, e28719 (2011).
15. Heins, N. *et al.* Glial cells generate neurons: the role of the transcription factor Pax6. *Nat. Neurosci.* **5**, 308–315 (2002).
16. Heinrich, C. *et al.* Directing astroglia from the cerebral cortex into subtype specific functional neurons. *PLoS Biol.* **8**, e1000373 (2010).
17. Heinrich, C. *et al.* Generation of subtype-specific neurons from postnatal astroglia of the mouse cerebral cortex. *Nat. Protoc.* **6**, 214–228 (2011).
18. Torper, O. *et al.* Generation of induced neurons via direct conversion in vivo. *Proc. Natl. Acad. Sci. USA* **110**, 7038–7043 (2013).
19. Su, Z., Niu, W., Liu, M.L., Zou, Y. & Zhang, C.L. In vivo conversion of astrocytes to neurons in the injured adult spinal cord. *Nat. Commun.* **5**, 3338 (2014).
20. Guo, Z. *et al.* In vivo direct reprogramming of reactive glial cells into functional neurons after brain injury and in an Alzheimer's disease model. *Cell Stem Cell* **14**, 188–202 (2014).
21. Heinrich, C. *et al.* Sox2-mediated conversion of NG2 glia into induced neurons in the injured adult cerebral cortex. *Stem Cell Reports* **3**, 1000–1014 (2014).
22. Torper, O. *et al.* In vivo reprogramming of striatal NG2 glia into functional neurons that integrate into local host circuitry. *Cell Rep.* **12**, 474–481 (2015).
23. Gascón, S. *et al.* Identification and successful negotiation of a metabolic checkpoint in direct neuronal reprogramming. *Cell Stem Cell* **18**, 396–409 (2016).
24. Brambrink, T. *et al.* Sequential expression of pluripotency markers during direct reprogramming of mouse somatic cells. *Cell Stem Cell* **2**, 151–159 (2008).
25. Esteban, M.A. *et al.* Vitamin C enhances the generation of mouse and human induced pluripotent stem cells. *Cell Stem Cell* **6**, 71–79 (2010).
26. Chambers, S.M. *et al.* Highly efficient neural conversion of human ES and iPS cells by dual inhibition of SMAD signaling. *Nat. Biotechnol.* **27**, 275–280 (2009).
27. Wernig, M. *et al.* Tau EGFP embryonic stem cells: an efficient tool for neuronal lineage selection and transplantation. *J. Neurosci. Res.* **69**, 918–924 (2002).
28. Kriks, S. *et al.* Dopamine neurons derived from human ES cells efficiently engraft in animal models of Parkinson's disease. *Nature* **480**, 547–551 (2011).
29. Pang, Z.P. *et al.* Induction of human neuronal cells by defined transcription factors. *Nature* **476**, 220–223 (2011).
30. Huang, T., Liu, Y., Huang, M., Zhao, X. & Cheng, L. Wnt1-cre-mediated conditional loss of Dicer results in malformation of the midbrain and cerebellum and failure of neural crest and dopaminergic differentiation in mice. *J. Mol. Cell Biol.* **2**, 152–163 (2010).
31. Huangfu, D. *et al.* Induction of pluripotent stem cells by defined factors is greatly improved by small-molecule compounds. *Nat. Biotechnol.* **26**, 795–797 (2008).
32. Pennarossa, G. *et al.* Brief demethylation step allows the conversion of adult human skin fibroblasts into insulin-secreting cells. *Proc. Natl. Acad. Sci. USA* **110**, 8948–8953 (2013).
33. Chung, T.L. *et al.* Vitamin C promotes widespread yet specific DNA demethylation of the epigenome in human embryonic stem cells. *Stem Cells* **28**, 1848–1855 (2010).
34. Liu, X. *et al.* Sequential introduction of reprogramming factors reveals a time-sensitive requirement for individual factors and a sequential EMT-MET mechanism for optimal reprogramming. *Nat. Cell Biol.* **15**, 829–838 (2013).
35. La Manno, G. *et al.* Molecular diversity of midbrain development in mouse, human, and stem cells. *Cell* **167**, 566–580.e19 (2016).
36. Koyano-Nakagawa, N., Kim, J., Anderson, D. & Kintner, C. Hes6 acts in a positive feedback loop with the neurogenins to promote neuronal differentiation. *Development* **127**, 4203–4216 (2000).
37. Jhas, S. *et al.* Hes6 inhibits astrocyte differentiation and promotes neurogenesis through different mechanisms. *J. Neurosci.* **26**, 11061–11071 (2006).
38. Dillon-Carter, O., Conejero, C., Tornatore, C., Poltorak, M. & Freed, W.J. N18-RE-105 cells: differentiation and activation of p53 in response to glutamate and adriamycin is blocked by SV40 large T antigen tsA58. *Cell Tissue Res.* **291**, 191–205 (1998).
39. Lundblad, M., Picconi, B., Lindgren, H. & Cenci, M.A. A model of L-DOPA-induced dyskinesia in 6-hydroxydopamine lesioned mice: relation to motor and cellular parameters of nigrostriatal function. *Neurobiol. Dis.* **16**, 110–123 (2004).
40. Darmopil, S., Muñetón-Gómez, V.C., de Ceballos, M.L., Bernson, M. & Moratalla, R. Tyrosine hydroxylase cells appearing in the mouse striatum after dopamine denervation are likely to be projection neurones regulated by L-DOPA. *Eur. J. Neurosci.* **27**, 580–592 (2008).
41. Masuda, M. *et al.* Postnatal development of tyrosine hydroxylase mRNA-expressing neurons in mouse neostriatum. *Eur. J. Neurosci.* **34**, 1355–1367 (2011).
42. Hu, G. *et al.* New fluorescent substrate enables quantitative and high-throughput examination of vesicular monoamine transporter 2 (VMAT2). *ACS Chem. Biol.* **8**, 1947–1954 (2013).
43. Freyberg, Z. *et al.* Mechanisms of amphetamine action illuminated through optical monitoring of dopamine synaptic vesicles in *Drosophila* brain. *Nat. Commun.* **7**, 10652 (2016).
44. Brooks, S.P. & Dunnett, S.B. Tests to assess motor phenotype in mice: a user's guide. *Nat. Rev. Neurosci.* **10**, 519–529 (2009).
45. Bagga, V., Dunnett, S.B. & Fricker, R.A. The 6-OHDA mouse model of Parkinson's disease - Terminal striatal lesions provide a superior measure of neuronal loss and replacement than median forebrain bundle lesions. *Behav. Brain Res.* **288**, 107–117 (2015).
46. Fasano, A., Aquino, C.C., Krauss, J.K., Honey, C.R. & Bloem, B.R. Axial disability and deep brain stimulation in patients with Parkinson disease. *Nat. Rev. Neurol.* **11**, 98–110 (2015).
47. Kurz, M.J. *et al.* A chronic mouse model of Parkinson's disease has a reduced gait pattern certainty. *Neurosci. Lett.* **429**, 39–42 (2007).
48. Bonito-Oliva, A., Masini, D. & Fisone, G. A mouse model of non-motor symptoms in Parkinson's disease: focus on pharmacological interventions targeting affective dysfunctions. *Front. Behav. Neurosci.* **8**, 290 (2014).
49. Amende, I. *et al.* Gait dynamics in mouse models of Parkinson's disease and Huntington's disease. *J. Neuroeng. Rehabil.* **2**, 20 (2005).
50. Wang, H., Li, X., Gao, S., Sun, X. & Fang, H. Transdifferentiation via transcription factors or microRNAs: current status and perspective. *Differentiation* **90**, 69–76 (2015).
51. Dickson, D.W. Parkinson's disease and parkinsonism: neuropathology. *Cold Spring Harb. Perspect. Med.* **2**, a009258 (2012).

## ONLINE METHODS

**Molecular cloning and viral production for *in vitro* experiments.** The plasmids Tet-O-FUW-Ascl1, Tet-O-FUW-NeuroD1 and Tet-O-FUW-GFP were cloned as previously described[7].

Lmx1a cDNA was amplified from an image clone (Open Biosystems) into Tet-O-FUW vector with EcoRI sites using primers with MfeI sites and incorporating a Kozak sequence:

Lmx1a Mfe1 Fwd:5′catg**CAATTG**GCCACCATGCTGGACGGCCTAAA GATG 3′

Lmx1a Mfe1 Rev: 5′ catg**CAATTG**TCAAGATGTGAAGTAAGAATTC 3′

NR4A2 cDNA was amplified from mouse embryonic e13.5 brain cDNA and cloned into the Tet-O-FUW vector containing a multiple cloning site using primers with XbaI and NheI sites and incorporating a Kozak sequence:

NR4A2 XbaI Fwd: 5′ catg**TCTAGA**GCCACCATGCCTTGTGTTCAGGC GCAG 3′

NR4A2 NheI Rev: 5′ catg**GCTAGC**TTAGAAAGGTAAGGTGTCCAGG 3′

The genomic sequence on mouse chromosome 5 containing miR218 was cloned into the lentiviral backbone Tet-O-FUW using the EcoR1 restriction site:

miR218 EcoR1 Fwd: 5′ ggcc**GAATTC**CCTCCCTTCGTCTTTCCT 3′

miR218 EcoR1 Rev: 5′ggcc**GAATTC**CCCCCAAAGCCTCTTTTAT 3′

The Tet-O-FUW-miR218, Tet-O-FUW-Ascl1, Tet-O-FUW-Lmx1a, Tet-O-FUW-NR4A2, Tet-O-FUW-NeuroD1, Tet-O-FUW-GFP and FUW-rtTA (Addgene 20342) lentiviruses were produced in HEK293FT packaging cells (Invitrogen) cultured in DMEM with 10% FBS and penicillin/streptomycin. On the day before the transfection, HEK293FT cells were plated in order to reach a 70–80% confluence on the next day. On the following day the cells were transfected using the XtremeGene9 transfection reagent (Roche) according to the manufacturer's instructions. The Tet-O-Fuw plasmids were individually co-transfected with the vectors pMDLg/pRRE (Addgene 12251), pRSV-Rev (Addgene 12253), and pMd2.G (Addgene 12259) in a 4:2:1:1 ratio, respectively. The transfection mix was removed after an overnight incubation, and fresh media were supplied to the cells. The volume of the fresh media was just sufficient to cover the cells and avoid their dehydration. 30 h after transfection, the media were collected and centrifuged for 5 min at 1,500 r.p.m. in order to separate the supernatant from cellular debris. Supernatants were then centrifuged for 2 h 30 min at 20,000*g* at 4 °C in a Beckman Coulter Avanti-J centrifuge. The resulting pellets were slowly resuspended in PBS over 2 h, then aliquoted and kept at −80 °C. Viruses were subsequently titrated using the Lenti-X Provirus quantitation kit (Clontech) in SVGp12 cells (ATCC) according to the manufacturer's instructions.

The pAAV5-FLEX-tdTomato (Addgene 28306) was used for tracing experiments.

**Cell culture and viral infection.** hIA were purchased from ATCC (SVGp12, cat. n CRL86-21) and hPA were purchased from Lonza (Normal Human Astrocytes, cat. n CC-2565). The cells were initially grown and amplified according to the manufacturer's instructions, and were used for experiments at low passages (maximum number of passages, four). Cells were chosen based on their inability to generate neurons in our control experimental conditions, indicating that they do not behave as stem/progenitor cells.

hIA were infected in their normal culture medium supplemented with 4 μg/ml of polybrene overnight, while hPA were infected in their normal culture medium overnight without polybrene.

**Basic protocol.** Following infection the cells were switched to fresh medium that was replaced every 2 d. After 5 d of amplification the expression of the transgenes was switched on by addition of doxycycline (2 μg/mL, Sigma). This doxycycline-supplemented medium was changed every other day until day the end of the experiment.

**Midbrain protocol.** Following infection the cells were switched to fresh medium containing ascorbic acid (50 μM, Sigma), SB431542 (10 μM, Tocris) and LDN193189 (0.5 μM, Stemgent) that was replaced every 2 d. After 5 d the expression of the transgenes was switched on by addition of doxycycline to the medium (2 μg/mL, Sigma). After 48 h the medium was changed to KON3 (KODMEM (Invitrogen), KSR 15% (Invitrogen) 25 μg/ml insulin (Sigma), 50 μg/ml transferrin (Sigma), 30 nM sodium selenite (Sigma), 20 nM progesterone (Sigma), 100 nM putrescine (Sigma) and 0.25% penicillin/streptomycin (Invitrogen)) containing doxycycline, CT99021 (1 μM, Tocris) and Shh (200 ng/mL, R&D). This medium was changed every other day until the end of the experiment.

**Remodeling TGFβ midbrain protocol.** Following infection the cells were switched to fresh medium that was replaced every 2 d. After 5 d the expression of the transgenes was switched on by addition of doxycycline (2 μg/mL, Sigma). After 24 h the medium was supplemented with TGFβ1 (3 ng/mL, Peprotech). 30 h later the medium was changed to KON3 containing doxycycline, ascorbic acid (150 μM), valproic acid (0.5 mM, Sigma) and 5-aza-2′-deoxycytidine (0.25 mM, Sigma).

After approximately 18 h the medium was changed to KON3 with doxycycline, ascorbic acid, SB431542 (2 μM, Tocris) and LDN193189 (0.25 μM, Stemgent). 30 h later the medium was changed to KON3 with doxycycline, ascorbic acid, CT99021 (0.6 μM, Tocris) and purmorphamine (0.5 μM, Stemolecule). This medium was changed every other day until day 13, after that time the cells were grown in KON3 with doxycycline only.

**Bulk RNA sequencing.** Library preparation was performed as previously described[52]. The analysis of differentially expressed genes was done using the DESeq2 package for R[53], using Wald test with a threshold at an adjusted *P*-value of 0.05. Genes expressed over basal levels in human postmitotic cells of the dopaminergic lineage (medial neuroblasts and DA neurons type 0, 1 and 2) during embryonic development[35] were used to define the mDA signature and to examine iDANs.

**Animals.** *B6.Cg-Tg*(*GFAP-tTA*)*110Pop/J* mice[54] were maintained in a 12-h light-dark cycle with food and water *ad libitum*. Experiments were carried out on adult mice between 2 and 6 months of age. Sample size was determined based on previous studies or preliminary data. Animals were weight-matched and randomly assigned to experimental groups. All experiments had received prior approval by the local animal ethical committee, Stockholms Norra Djurförsöksetiska Nämnd (N273/11; N326/12; N114/15; N158/15), and were carried out in accordance with the European Community Council Directive of 24 November 1986 (86/609/EEC).

In order to report iDAN reprogramming, heterozygous *B6.Cg-Tg*(*GFAP-tTA*)*110Pop/J* mice were bred with homozygous $DAT^{Cre/+}$ mice[55] crossed with $Rosa26R^{Tomato}$ mice (Jackson). Triple heterozygous offspring were used for the experiments.

**6-OHDA lesion.** For dopamine depletion in the right striatum, mice received a unilateral injection of 6-hydroxydopamine-HCl (6-OHDA-HCl) into the right medial forebrain bundle (MFB). All animals received subcutaneous injections of Temgesic as analgesic at a dose of 0.1 mg/kg before the surgical procedure. Anesthesia was induced with 4% isofluorane, and maintained with 2% isoflurane. The mouse was positioned in a stereotaxic frame (David Kopf Instruments, Tujunga, CA) on a heating pad to maintain normothermia. 6-OHDA-HCl (Sigma-Aldrich, Sweden AB) was dissolved in 0.02% ascorbic acid in saline at a concentration of 3.75 μg of free-base 6-OHDA/μL. Each mouse was injected with 1 μl (0.2 μl/min) of solution into the right MFB according to the following coordinates (mm): anteroposterior (AP), −1.2; mediolateral (ML), −1.2; dorsoventral (DV), 4.8 (all millimeters relative to bregma). The needle was left in place for 5 min before and after injection. Mice were allowed to recover for 2 weeks before experimentations.

**Stereotaxic injections.** Dopamine-depleted *GFAP-tTA* mice were injected in the right striatum with high-titer lentiviruses or adeno-associated virus (AAV) that were produced at the University of North Carolina Vector Core Facility. Mice were anesthetized with isofluorane and secured in a stereotaxic frame as during the 6-OHDA lesion procedure. Each mouse received one injection of 1.5 or 2 μl (0.1 μl /min) into the right dorsal striatum, according to the following coordinates for single injection (mm): AP, +1; ML, −2; DV, −3.5; or for the high-dose NeAL218 double injection site (mm): AP, +1 and 0.3; ML, −2; DV, −3.5, (all millimeters relative to bregma). The needle was left in place for 5 min before and 15 min after the delivery of the viral vector.




doi:10.1038/nbt.3835

**Perfusion.** Mice were deeply anesthetized with sodium pentobarbital (200 mg/kg, intraperitoneally (i.p.), Sanofi-Aventis, France) and perfused transcardially with 4% (weight/vol) ice-cold paraformaldehyde (PFA) in 0.1 M PB.

**Treadmill gait analysis.** The gait analysis was carried out with ventral plane videography. Mice were placed in a rectangular plexigas-testing chamber (20 × 5 × 17 cm) mounted over a motorized transparent treadmill (Exer Gait XL, Columbus Instruments, USA). Digitalized videos (658 × 494 pixels at 100 frames/sec) of the bottom view were collected with an angled mirror (45 degrees) mounted directly below the testing chamber. Each mouse was placed into the testing chamber and the treadmill was turned on and operated at the set speed (17 cm/s). Mice were recorded for a preset fixed number of 2,000 frames after which the treadmill was stopped. Every mouse was filmed during three trials separated by 1-min inter-trial periods. From the videos, each digitalized paw-treadmill contact was time-stamped and gait was analyzed. Additional kinematic and postural measurements were derived from relative body-to-paw distances. The following standard gait parameters were presented: gait cycles (sequence of paw placement over time), sagittal symmetry (the distance between front left and rear left paw in relation to front right and rear right paw) and paw coordination index (or phase value is essentially the alternation between two limbs). The time during which the animals run to the front, drifted backward on the belt, or explored the chamber were excluded from the analysis. Outcome assessment was done with an investigator who was blinded to sample identity. Prism 5 (GraphPad) and Treadscan (Treadscan 4.0, Clever Sys, Inc., Reston, VA, USA) were used for statistics and graphing.

Quantification of various parameters submitted to gait analysis with a minimum of 100 steps/paw. Data were analyzed using one-way ANOVA followed by Dunnett's *post hoc* multiple comparisons test. Whenever data deviated from normality, groups were compared with Kruskal–Wallis followed by Dunn's *post hoc*. Student's *t*-test was used to analyze parameters within two groups. A probability value of ≤0.05 was used as a limit for declaring statistical significance.

**Drug-free and drug-induced rotation analyses.** Mice were placed in cylinders (diameter 12.5 cm and height 30 cm). The experiments were recorded from a ventral plane view to avoid wall shadowing. Rotations in drug-free condition were monitored for 15 min. For drug-induced rotations the mice were allowed to habituate for 15 min and monitored for 45 min, starting 10 min after injection of D-amphetamine (Sigma, 5 mg/kg, i.p.) or apomorphine hydrochloride (Sigma, 5 mg/kg, s.c.). Videos were analyzed with automated full-body rotation counts using Ethovision software (Ethovision XT 11), for which the configurations were compared to scoring performed by an observer during experimental setup.

Mice were given 4 weeks to recover, following each D-amphetamine injection, and 4 d between apomorphine and D-amphetamine test on week 13, to ensure drug washout before behavioral testing. Net rotations were calculated based on the direction of the majority of the turns (i.e., net ipsilateral = total right − total left 360° turns and net contralateral = total left − total right 360° turns) and were expressed as net rotations/min for drug-induced ipsilateral or contralateral rotations (**Fig. 5a**), or net rotations/15 min for spontaneous ipsilateral rotations (**Fig. 5b**).

**Immunocytochemistry and immunohistochemistry.** For immunocytochemical analysis, cells were fixed for 20 min at room temperature in 4% paraformaldehyde (PFA) in PBS, permeabilized and blocked for 60 min in PBS containing 0.3% Triton X-100, 0.1% BSA and 5% normal donkey serum (PBTA-NDS). Then they were incubated overnight at 4 °C in PBTA-NDS with the appropriate primary antibodies. The cells were then washed three times with PBS and incubated for 1 h at room temperature with Alexa Fluor secondary antibodies (1:1,000, Invitrogen) in PBTA-NDS.

For immunohistochemical analysis adult mice were perfused with ice cold 4% PFA and the brains were postfixed at 4 °C with 4%PFA. After 18 h the brains were washed in PBS 3 times for several hours and put in sucrose 15%, then sucrose 30% in PBS until they sank, to be then embedded in OCT. Frozen brains were sectioned into 14-µm-thick sections with a cryostat and processed for immunostaining or kept at −20 °C. Sections were permeabilized for 1 h at room temperature in PBTA-NDS and incubated overnight at 4 °C in PBTA-NDS containing the primary antibodies. Sections were then washed three times with PBS-Tween 0.5% and incubated for 1 h at room temperature with Alexa Fluor secondary antibodies (1:1,000, Invitrogen) in PBTA-NDS. Microphotographs were taken with a Zeiss LSM700 confocal microscope or an Olympus FV1000 confocal microscope and images were analyzed with the ImageJ 1.48 g software for Windows. In some cases the "smooth" process was applied to the entire image on all visible channels, in order to make the image clearer to the viewer.

Primary antibodies: rabbit anti-TH (1:400, Pel-Freez, P40101-0), mouse anti-TH (1:250, Immunostar, 22941), sheep anti-TH (1:250, Novus Biologicals, NB300-110), mouse anti-TUBB3 (1:300, Promega, G712A), mouse anti-MAP2 (1:50, Sigma, M4403), rat anti-SLC6A3 (1:100, Abcam, ab5990), rabbit anti-DDC (1:100, Novus Biologicals, NB 300-252), goat anti-KCNJ6 (1:100, Novus Biologicals, NB 100-74575), rabbit anti-KCNJ6 (1:100, Alomone Labs, APC006), mouse anti-SYN1 (1:200, Biogenesis), goat anti-GFP-FITC (1:1,000, Abcam, ab6662), rabbit anti-ALDH1A1 (1:200, Abcam, ab23375), rabbit anti-RBFOX3 (1:500, Millipore, MAB377), goat anti-DCX (1:400, Santa Cruz, sc-8066 ), rabbit anti-PBX1 (1:200, Santa-Cruz, sc-101851), rabbit anti-NR4A2 (1:200, Santa-Cruz, sc-990).

**Cell counting.** The percentages of $TH^+$ neurons over DAPI in *in vitro* experiments were quantified after 10 d of doxycycline induction. $TH^+$ neurons were counted manually and $DAPI^+$ nuclei were counted automatically with the IMARIS software v 7.5. For each condition several randomly picked fields were photographed with a 10× objective on a confocal microscope from 48-well plates. The total number of $TH^+$ neurons for each condition was normalized with the total number of nuclei per condition. The numbers of $Map2^+$ neurons were counted in the same way and normalized over the number of $TH^+$ neurons per condition.

The numbers of $TH^+$ cells in adult mouse striata were quantified by counting all the $TH^+$ cells present in the right striatum from bregma 0.36 to bregma +1.4, in 14-µm-thick sections at 140-µm intervals, only cell bodies in which the nucleus was clearly visible were counted. The counted sections represent ~10% of all the sections ranging from bregma 0.36 to bregma +1.4.

Outliers were detected by using the absolute deviation from the median, statistical significance was measured with the Student's *t*-test (unpaired and with unequal sample variance, $*P \leq 0.05$; $**P \leq 0.01$).

**RT–qPCR.** RNA was extracted using miRNeASY microRNA isolation system (Qiagen) according to the manufacturer's instructions and treated with DNAse on-column protocol. 100–500 ng of total RNA containing miRs were reverse-transcribed using the Superscript II kit (Invitrogen). The reverse-transcribed cDNA was amplified using Fast SYBRGREEN (Applied Biosystems) in a StepONE plus real time-qPCR machine (Applied Biosystems). Outliers were detected by using the absolute deviation from the median, statistical significance was measured with the Student's *t*-test (unpaired and with unequal sample variance, $*P \leq 0{,}05$; $**P \leq 0{,}01$).

**Electrophysiology and calcium imaging of cells.** Human astrocytes were assayed with the patch-clamp technique using the whole-cell configuration. Cells for recording were preselected based on morphological criteria typical for neurons such as the presence of projections and a non-flattened cell body. Ion currents and membrane potential were recorded, filtered, and analyzed using an Axopatch 200 B amplifier, a DigiData1322 interface, and the pClamp10 software, respectively (Molecular Devices). Intracellular solution contained 114 mM K-gluconate, 6 mM KCl, 10 mM HEPES, 5 mM EGTA, 4 mM ATP-Mg and 0.3 mM GTP (pH was adjusted to 7.3 with KOH). For calcium imaging the coverslips with cells were preloaded with 4 mM Fluo-4AM (Invitrogen) for 20–30 min at 37 °C. Ratiometric imaging was performed on a CoolSnap $HQ^2$ camera (Photometrics) and analyzed by MetaFluor software (Molecular Devices). The bath solution for electrophysiological recordings and calcium imaging contained (mM) 140 NaCl, 2.5 KCl, 1 $MgSO_4$, 1.3 $CaCl_2$, 1.2 $NaH_2PO_4$, 10 glucose and 10 HEPES–NaOH, pH 7.4. Statistical analysis was done with Mann-Whitney Rank Sum Test. $*P < 0.05$.

**Brain slices electrophysiology and FFN206 live imaging.** Adult mice were deeply anesthetized (5% isoflurane) and perfused with 40 ml ice-cold pre-oxygenated (95% $O_2$/5% $CO_2$) cutting solution containing (in mM): 90 NaCl,

26 $NaHCO_3$, 2.5 KCl, 1.2 $NaH_2PO_4$, 10 HEPES-NaOH, 5 Na-ascorbate, 5 Na-pyruvate, 0.5 $CaCl_2$, 8 $MgSO_4$ and 20 glucose). Then brains were rapidly extracted and immersed in the same solution. Subsequently, 250-µm-thick coronal slices were cut on a vibratome (VT1200S, Leica). Slices encompassing the striatum were selected and equilibrated in artificial cerebrospinal fluid (ACSF) containing (in mM): 124 NaCl, 26 $NaHCO_3$, 2.5 KCl, 1.2 $NaH_2PO_4$, 2 $CaCl_2$ and 2 $MgSO_4$ at 22–24 °C for 1–4 h before recording. Whole-cell recordings in current-clamp or voltage-clamp mode were made by using MultiClamp amplifier, a DigiData1440 interface, and the pClamp10 software (Molecular Devices). During measurements, slices were continuously perfused with ASCF. The internal pipette solution contained (in mM): 114 K-gluconate, 6 KCl, 10 HEPES, 5 EGTA, 4 ATP-Mg, 0.3 GTP (pH was adjusted to 7.3 with KOH). After recordings, brain slices were immersion fixed with 4% PFA at 4 °C overnight. Electrophysiological data were analyzed using Clampfit 10.0 (Molecular Devices) and SigmaPlot (Systat Software Inc.).

For live imaging, after equilibration in ACSF, the slices were incubated 30 min in the dark in ACSF containing 10 µM FFN 206 (Abcam), then washed for 30 min in the dark in ACSF.

Slices were imaged on a Zeiss LSM700 confocal, and FFN206 release was induced by addition on the slice of KCl 56 mM (final concentration).

**Statistics.** *Cell quantification.* For $TH^+$ and $TH^+$; $MAP2^+$ cells in *in vitro* experiments, replicates are counts in independent experiments performed in duplicate. Data are expressed as box plots showing the median as well as the 25th and 75th percentiles.

*Transcriptomics data.* Replicates are independent experiments; for human VM, hIAs at day 0 and hIDANs at day 10 $n = 4$.

*Electrophysiological data.* Replicates are individual cells recorded over several independent experiments. Data are presented as box plots with the median, 10th, 25th, 70th and 90th and percentiles.

*Gene expression data.* Replicates are independent experiments. Data in Figure 2e are expressed as box plots showing the median as well as the 25th and 75th percentiles. Significance measured with two-tailed Student's *t*-test with unequal sample variance. For **Figure 2e**, all genes in untreated cells, $n = 7$; *NRA4A2*, *PITX3*, *SLC18A2*, *SLC6A3*, *KCNJ6* in MP $n = 3$; *ALDH1A1*, *CALB1* in MP $n = 4$; *EN1* and *FOXA2* in MP $n = 5$; *EN1*, *FOXA2*, *SLC6A3* in RTMP $n = 3$; *SLC18A2*, *CALB1*, *KCNJ6* in RTMP $n = 4$; *NR4A2*, *PITX3*, *ALDH1A1* in RTMP $n = 5$.

*Confocal images.* Images reported in **Figure 1d** in basic protocol are representative images chosen from the results obtained in 4 independent experiments. Confocal images reported in **Figure 1d**, **Supplementary Figure 1a**,**b** in midbrain protocol are representative images chosen from the results obtained in 3 independent experiments. Confocal images reported in **Figure 1g** at 10 d are representative images chosen from the results obtained in 7 independent experiments. Confocal images reported in **Figure 1g** at 17 d are representative images chosen from the results obtained in 3 independent experiments. Confocal images reported in **Figure 2b** are representative images chosen from the results obtained in 7 independent experiments Confocal images reported in **Figure 2k** and **Supplementary Figure 3b** are representative images chosen from the results obtained in 5 independent experiments. Confocal images at 2 weeks reported in **Figure 3d** and **Supplementary Figure 4b,c** are representative images chosen from the results obtained in 8 animals (NeAl218 $n = 4$, GFP $n = 4$). Confocal images at 13 weeks reported in **Figure 3c**,**d**,**e** and **Supplementary Figure 4a,d** are representative images chosen from the results obtained in 26 animals (NeAl218 $n = 13$, GFP $n = 13$). Confocal images reported in **Figure 4a–d** and **Supplementary Fig. 4e**,**f** are representative images chosen from the results obtained in 7 animals (NeAl218 $n = 5$, GFP $n = 2$). Confocal live black and white images reported in **Figure 4c** and **Supplementary Figure 5b** are representative images chosen from the results obtained in 8 animals (NeAl218 $n = 4$, control $n = 4$).

*Behavioral data.* Replicates are individual animals analyzed over several independent experiments.

**Data availability.** Sequencing data of hIAs, hIDANs and hVM: GSE93528.


52. Zeisel, A. *et al.* Brain structure. Cell types in the mouse cortex and hippocampus revealed by single-cell RNA-seq. *Science* **347**, 1138–1142 (2015).
53. Love, M.I., Huber, W. & Anders, S. Moderated estimation of fold change and dispersion for RNA-seq data with DESeq2. *Genome Biol.* **15**, 550 (2014).
54. Wang, J., Lin, W., Popko, B. & Campbell, I.L. Inducible production of interferon-gamma in the developing brain causes cerebellar dysplasia with activation of the Sonic hedgehog pathway. *Mol. Cell. Neurosci.* **27**, 489–496 (2004).
55. Ekstrand, M.I. *et al.* Progressive parkinsonism in mice with respiratory-chain-deficient dopamine neurons. *Proc. Natl. Acad. Sci. USA* **104**, 1325–1330 (2007).





doi:10.1038/nbt.3835